Nanoscale Optical Channel Modeling for *In Vivo* Wireless Nanosensor Networks: A Geometrical Approach

Pedram Johari and **Josep Miquel Jornet**
Department of Electrical Engineering, University at Buffalo, The State University of New York
Buffalo, NY 14260, USA. E-mail: {pedramjo, jmjornet}@buffalo.edu.

***Abstract*—*In vivo* Wireless Nanosensor Networks (iWNSNs) consist of nano-sized communicating devices with unprecedented sensing and actuation capabilities, which are able to operate inside the human body. Major progress in the field of nanoelectronics, nanophotonics and wireless communication is enabling the communication among nanosensors. Among others, plasmonic nanolasers with sub-micrometric footprint, plasmonic nano-antennas able to confine light in nanometric structures, and single-photon detectors with unrivaled sensitivity, enable the communication among implanted nanosensors in the near infrared and optical transmission window. In this paper, a channel model for *in vivo* optical communication in iWNSNs is developed. By following a geometrical approach to trace and aggregate the path loss and time delay of each of the rays that encounter a biological cell, a closed form channel impulse response is derived. The analytical channel model is validated by means of electromagnetic simulations for a Red Blood Cell (RBC) inside the blood plasma. The results show that RBCs perform as optical micro-lenses in terms of confining the light that is being radiated to them on a focal line right after the cell. This results are in strong agreement with the recent experimental achievements on interactions of light and RBCs.**

I. Introduction

Major breakthroughs in the field of nano-bio-photonics are enabling the control and monitoring of biological processes through light. For example, by incorporating light-actuated/light-emitting proteins into cells, key biological processes can be controlled and monitored in real time [1], [2]. While the very small wavelength of optical signals theoretically enables such precise temporal and spatial control and monitoring, currently, all the existing studies rely only on traditional optical sources and detectors, which, due to their size and capabilities, limit the applications of light-mediated bio-interfaces. In parallel to such developments, nanotechnology is providing the engineering community with a new set of tools to create novel nanoscale devices with unprecedented functionalities. These include, among others, plasmonic nano-lasers with sub-micrometric footprint [3], plasmonic nano-antennas able to confine light in nanometric structures [4], or single-photon detectors with unrivaled sensitivity [5]. Plasmonic nano-lasers working in conjunction with nano-antennas can serve as nano-actuators of light-controlled processes. Similarly, nano-detectors enhanced with plasmonic nano-antennas can act as nanosensors.

By means of communication, these nano-actuators and nanosensors will be able to autonomously transmit their sensing information to common sink, be controlled from a command center, or coordinate joint actions when needed. The resulting *in vivo* Wireless NanoSensor Networks (iWNSNs) enable smart health-monitoring and drug-delivery systems, and many other applications. Among several wireless technologies that could enable the communication between nanomachines, the molecular and electromagnetic communications are the leading ones. The molecular communication is currently being thoroughly investigated [6]. Although this mechanism is naturally used by cells to exchange information and could be enabled by means of synthetic biology, the very low achievable data rates drastically limit the usefulness of nanosensor networks [7]. From the electromagnetic perspective, emerging plasmonic nanoantennas have been recently enabled the wireless communication among nano-devices at very high frequencies, ranging from the Terahertz (THz) band (0.10-10 THz) to the infra-red and visible optical range [4], [8]. The propagation of THz-band waves inside the human body is drastically impacted by the absorption of liquid water molecules. Indeed, THz radiation, while non-ionizing, induce internal vibrations into molecules, which results in heat and could lead to thermal tissue damage. Alternatively, it is well known that the molecular absorption of liquid water is minimal in the optical window, between 400 THz and 750 THz [9]. This is the reason why the majority of existing nano-bio-sensing technologies rely on the use of light.

In order to analyze the feasibility of intra-body wireless optical communications, it is necessary to understand the propagation properties of light in biological scenarios. Existing channel models for light propagation in biological tissues [10–12] cannot directly be utilized because of several reasons. For one thing, in intra-body NanoScale Optical (NSO) communications the wavelength range of study is in the order of several hundreds of nanometers. Therefore, due to the short range distances and relatively large particles -compared to the wavelength-, the macroscopic properties of different particles cannot accurately describe the propagation pattern of the light. Moreover, the light radiated from a nano-antenna covers a much smaller area than that of the external macroscopic laser; hence, the number of cells that the wave radiates through is not large enough to be dealt with as an isotropic medium. Therefore, the need to analyze the impact of single cells rather than a homogeneous material to study the propagation pattern of the wave and develop the channel model for intra-body NSO communications is clear. We have investigated the impact of

978-1-4673-8999-0/17/$31.00 ©2017 IEEE

single cells in a preliminary work [13], in which an analytical model in frequency domain is given. However, the effect of the geometry on focusing the light, attenuation of the light intensity, and time delay of individual optical rays that are passing through the cell has not been considered.

In this paper, we develop a channel model for *in vivo* optical communication in iWNSNs. In particular, due to the rather large size of the biological cells compared to the wavelength, we follow a geometrical approach to trace path loss and time delay of each of the rays that encounter a biological cell. A closed form channel impulse response on the focal line is derived by aggregating all the rays while considering the attenuation and delay of each of them. We show that after passing a single Red Blood Cell (RBC), all the optical rays will be focusing on the central line. In fact, it causes RBCs to perform as optofluidic micro-lenses inside the human blood which has also recently been experimentally proved [14]. The final propagation pattern that has been derived for a single cell can be further used to model more complex channels including numerous cells of different types in multiple layers for more realistic *In vivo* optical communications.

The remainder of the paper is organized as follows. In Sec. II, we define the cell model, and further study the interaction of light and biological tissues. Sec. III contains a geometrical approach to thoroughly analyze the propagation of the light through the cell by tracing all the incident light rays. In Sec. IV, we numerically study the geometrical channel model and compare the model with multiphysics simulations. Finally, we conclude the paper in Sec. V.

II. System Model

A. Cell Model

Different types of cells affect the propagation of light in different ways. In this work, we focus on light propagation in blood vessels. Human blood is composed by erythrocytes (RBCs), leukocytes (white blood cells), and thrombocytes or Platelets. Among all these, RBCs are the largest (7 microns) and most abundant (45%) and, thus, govern the propagation of light in blood. All the blood cells are floating inside the blood plasma (55% of blood) which is essentially water (92%).

Therefore, in our scenario, we consider RBCs immersed in plasma. Plasma is modeled as a lossy medium with macroscopic properties (mainly the complex permittivity) of the water which captures the effect of the medium on the optical propagating wave. Each RBC is modeled as a multi-layered sphere, with the outer shell as the cell membrane, filled with the cytoplasm and the nucleus (hemoglobin for RBC). The spherical cell is widely used in simulation and analytical researches [10–12]. However, the shape of different cells are not necessarily spherical, and the nucleus is not always at the center of it. Nonetheless, the sphere is a general model that is used as a good approximation for all types of cells with different shapes due to the random positions and movement of the cells in different layers of biological tissues. As depicted in Fig. 1, a typical RBC has three layers: Innermost layer is hemoglobin with complex permittivity ϵ_1 and radius r_1; Intermediate layer is cell cytoplasm with complex permittivity ϵ_2 and radius r_2; Outermost layer is cell membrane (mainly fat) with complex permittivity ϵ_3 and radius r_3.

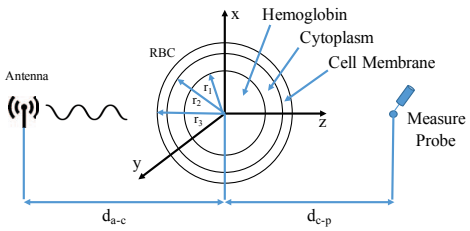

Fig. 1. Red Blood Cell Model.

B. Light and Biological Tissues Interactions

The radiation of the light in a medium is mainly affected by reflection, refraction, diffraction, and scattering. The diffraction and scattering happen when the wavelength of the incident light is comparable to the size of the particle, while the refraction and reflection are related to the intrinsic properties of the materials and are studied in geometric optics.

1) Diffraction: Diffraction occurs when the light encounters a very small obstacle (on an edge or a material with a coarse surface) or passes through a tiny aperture. Hence, the effect of diffraction is negligible in our analysis of shining light through a single smooth shaped and large (in comparison with wavelength) biological cells in a homogeneous medium.

2) Scattering: For the scattering there are three different major theories to analyze the way that the wave deviates from a straight trajectory based on the size of the particle that it encounters. A dimensionless size parameter is defined by the ratio of the characteristic particle diameter to the wavelength $\chi = \frac{\pi D}{\lambda/n_r}$, where D is the diameter of the particle, λ represents the wavelength in vacuum and n_r is the real part of the refractive index of the medium. Based on the value of the size parameter χ, the scattering model is categorized in three groups, namely, Rayleigh scattering for $\chi \ll 1$, Mie scattering for $\chi \approx 1$, and geometric scattering for $\chi \gg 1$.

In case of the propagation of light inside the human blood, with normal and healthy RBCs, the size parameter is around $\chi = 49$ for a wavelength of 600 nm and refractive index of $n_r = 1.33$ for the blood plasma, which assures the geometrical approach to be an accurate enough approximation.

3) Refraction: Refraction of the light in absorbing materials is described by using the refractive index $n(w) = \sqrt{\mu_r(w)\epsilon_r(w)}$, which is a complex-valued number and depends on the frequency w or equivalently the wavelength. ϵ_r is the relative permittivity, and μ_r is the relative permeability of the material. The real part of the refractive index accounts for the refraction, while the imaginary part deals with the absorption and is sometimes referred to as extinction coefficient.

While the refractive index is used for geometric optics analysis in Fresnel equations and Snell's law, the permittivity and permeability are useful in Maxwell's equations and electromagnetic radiation of the waves (used in simulation results presented in Sec. IV). Since the biological tissues are non-magnetic at the optical frequencies, the value of μ_r is considered to be equal to one. Therefore the real and imaginary parts of the refractive index and the relative permittivity are related to each other through $\epsilon_{r,r}(w) = n_r^2(w) - n_i^2(w)$ and $\epsilon_{r,i}(w) = 2n_r(w)n_i(w)$. Where subscripts r and i represent the real and imaginary parts of parameters.

4) Reflection: When light passes from one medium to another with two different refractive indexes, both reflection and refraction may occur. The Fresnel's equations describe what portion of the light is reflected and what portion is refracted (transmitted). The fat tissue (the outermost layer of RBC) causes the backscattered light by reflecting back a part of the incident light. However, the reflection does not play a significant role to form the impulse response of the channel on the focal line after the cell, and the received signal mainly consists of the refracted and transmitted rays.

III. Geometrical Analysis for Light Propagation through Biological Cells

Geometrical analysis of the light propagation, also known as Ray Optics, is the limit of Maxwell's equations when wavelength is small comparing to the size of particles, and is much tractable to obtain a closed form solution.

Fig. 2 shows the the trace of a ray while passing through a sphere with a different refractive index. Due to the symmetry in the geometry we know that all rays of the incoming light (considered to be a plane wave) will be focused on the central line that is coming out from the cell. For this reason we are mostly interested to find the impulse response on this specific focal line. Considering a linear channel, if a single pulse is being transmitted from the antenna, we will receive multiple versions of the same pulse spread in time due to different paths that the light rays experience. Therefore, the impulse response of the channel includes different delayed pulses (and hence a phase shift) from all incoming rays of light. To find the impulse response at a point on the focal line, we have to calculate: The location of focal point on the central line according to the incoming ray, $r \cdot f(\alpha)$ (Fig. 2); Path loss of each of the rays that pass the focal point, and the intensity and direction of received signal, E_F; Time (or the delay) between the transmitted and each of the received rays at that point, τ.

As it can be seen in Fig. 2, there is a main ray that passes through the center of the cell and over the entire focal line E_F^{mr}. In addition to that, there are other rays of light that encounter refraction and pass through the cell and the focal line at a certain point ($r \cdot f(\alpha)$ from the center of the cell), and we call them the secondary (focusing) rays E_F^{fr}. A complete trace of a single secondary ray is shown in Fig. 2, which is in a distance d_r from the central line. If we cover all the rays that are corresponded to $0 < \alpha < 1$ -the upper half of the cell-, then by taking the integral of the received signal over θ, which is the angle between the plane of incident and the x axis in the spherical coordinates, we can find the complete answer for each point on the focal line.

When a trace of light passes through a layer with a different refractive index and goes further through the same medium, the angle of the output ray is the same as the input one, and it only shifts proportionally to the thickness of the layer in between. Therefore, since we consider the refractive index of the blood plasma and the cell cytoplasm to be the same, so the effect of the thin fat layer of the RBC is only to shift the ray of the light very slightly. Also the absorption and the time delay due to this thin layer is negligible and can be ignored in calculation of the channel impulse response.

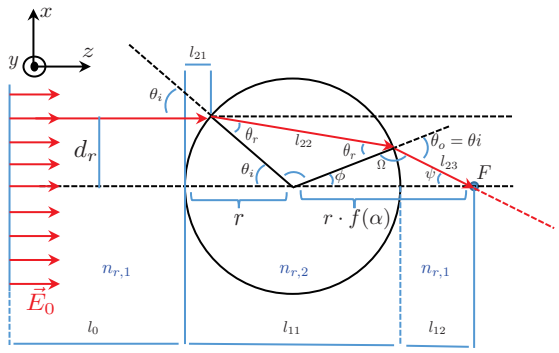

Fig. 2. Effect of the Hemoglobin as a spherical lens.

A. Focus Point

To find the focus point in Fig. 2, we define α as the ratio of d_r to r, where d_r is the distance between the ray and the central axis of the sphere, and r is the radius of the sphere. From the Snell's law of refraction we have $n_{r,2}sin(\theta_r) = n_{r,1}sin(\theta_i)$, where $n_{r,1}$ and $n_{r,2}$ are the real part of the refractive index of the medium and the cell respectively, and θ_i and θ_r are the incident and refracted angles. The refracted angle inside the sphere can be derived as follows:

$$\theta_r = arcsin\Big(\frac{n_{r,1}}{n_{r,2}} sin(\theta_i)\Big). \tag{1}$$

Since $sin(\theta_i) = d_r/r$, we can further obtain $\theta_i = arcsin(\alpha)$ and $\theta_r = arcsin(\frac{n_{r,1}}{n_{r,2}}\alpha)$. We are interested in finding $f(\alpha)$ to obtain the focus point F (Fig. 2). Following the Sine rule for triangles we have:

$$\frac{r \cdot f(\alpha)}{sin(\Omega)} = \frac{r}{sin(\psi)}. \tag{2}$$

By exploiting some simple trigonometric rules, and the facts that $\psi = 2\theta_i - 2\theta_r$, and $\Omega = \pi - \theta_i$, and using the definitions of θ_i and θ_r, $f(\alpha)$ in (2) can be further calculated as follows:

$$f(\alpha) = \frac{\alpha}{sin\Big[2\Big(arcsin(\alpha) - arcsin(\frac{n_{r,1}}{n_{r,2}}\alpha)\Big)\Big]}. \tag{3}$$

It can be observed that the value of the $f(\alpha)$ only depends on the ratio between the refractive indeces of the media, i.e., $\frac{n_{r,1}}{n_{r,2}}$, and regardless of the size of the cell, the ratio of the focus point to the radius of the cell remains unchanged. Also, the value of α is always between 0 and 1 for the plane optical wave source that is emitting through the sphere, and is polarized along x axis. The focus point always lies in between the upper and lower bounds of the function $f(\alpha)$ multiplied by the radius of the cell r. The lower bound of the function $f(\alpha)$ can be calculated as follows:

$$f_l = f(\alpha)\Big|_{\alpha=1} = \frac{1}{sin\Big[2\Big(\frac{\pi}{2} - arcsin(\frac{n_{r,1}}{n_{r,2}})\Big)\Big]}, \tag{4}$$

which can be further simplified to:

$$f_l = \frac{n_{r,2}^2}{2n_{r,1}\sqrt{n_{r,2}^2 - n_{r,1}^2}}. \tag{5}$$

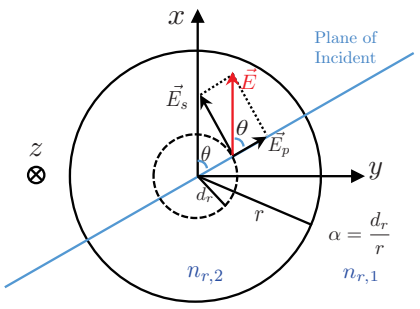

Fig. 3. Polarization of the light wave for different planes of incident with different θ ranging from 0 to 2π.

For the upper bound we have:

$$f_u = f(\alpha)\Big|_{\alpha=0} = \frac{0}{sin\Big[2\Big(arcsin(0) - arcsin(0)\Big)\Big]}, \quad (6)$$

where the equation (6) is indeterminate. Therefore, to find the upper limit, we find the limit of $f(\alpha)$ as α approaches zero, using $L'H\hat{o}pital's$ rule as follows:

$$\begin{aligned} f_u &= \lim_{\alpha\to 0} f(\alpha) \\ &= \frac{\left(\frac{1}{\sqrt{1-\alpha^2}} - \frac{\frac{n_{r,1}}{n_{r,2}}}{\sqrt{1-\frac{n_{r,1}^2}{n_{r,2}^2}\alpha^2}}\right)^{-1}}{2cos\Big[2\Big(arcsin(\alpha) - arcsin(\frac{n_{r,1}}{n_{r,2}}\alpha)\Big)\Big]}\Bigg|_{\alpha=0}, \end{aligned} \quad (7)$$

which can be further simplified to:

$$f_u = \frac{n_{r,2}}{2(n_{r,2} - n_{r,1})}. \quad (8)$$

B. Time Delay for Different Rays of the Wave

The time delay for the main ray on the focal line can be calculated by adding all the partial times that takes for the light to pass through different parts of the path in different media $\tau_{mr} = (l_0 n_{r,1} + l_{11} n_{r,2} + l_{12} n_{r,1})/c$, where c is the speed of light in vacuum, l_0 is the distance between the source and the cell boundary, $l_{11} = 2r$, and $l_{12} = r \cdot (f(\alpha) - 1)$. The delay for an arbitrary secondary (focusing) ray on the focal line is $\tau_{fr} = (l_0 n_{r,1} + l_{21} n_{r,1} + l_{22} n_{r,2} + l_{23} n_{r,1})/c$, where l_{21}, l_{22}, and l_{23} are given as follows by using the Sine law:

$$l_{21} = r\big(1 - cos(\theta_i)\big), \quad (9)$$

$$l_{22} = r\Big(\frac{sin(2\theta_r)}{sin(\theta_r)}\Big), \quad (10)$$

$$l_{23} = r\Big(\frac{sin(2\theta_r - \theta_i)}{sin(2\theta_i - 2\theta_r)}\Big). \quad (11)$$

Since θ_i and θ_r can be calculated from α, it can be seen that the time delay also only depends on the real part of the refractive index, the parameter α, and the cell radius r.

C. Path Loss and the Light Intensity on the Focal Line

To find the intensity of the light at a point on the focal line, we calculate the path loss of all the rays that are passing this line. By aggregating all the rays that pass the same point and including the delay for each ray form Sec. III-B, we will be able to find the channel impulse response at the desired point.

There are three different losses that have to be considered, namely, the molecular absorption loss $\mathcal{L}_{abs}$, the scattering loss $\mathcal{L}_{sca}$, and the boundary loss $\mathcal{L}_{bound}$. Due to the fact that we are considering a plane wave as the emitting light source, there will be no spreading loss caused by the antenna propagation pattern. Note that in the case of using a directional or omni light source the spreading loss also has to be considered. The molecular absorption loss in different media according to the Beer-Lambert law is given by $\mathcal{L}_{abs} = e^{-\mu_{abs} l}$, where l is the distance that the wave passes, $\mu_{abs} = 4\pi n_i(w)/\lambda$ is the absorption coefficient of the medium.

The attenuation due to the scattering can also be represented as an exponential loss $\mathcal{L}_{sca} = e^{-\mu_{sca} l}$, where μ_{sca} is the scattering coefficient of the medium and is given by $\mu_{sca} = NQ_{sca}\sigma_g$, where N is the particle concentration, σ_g is the geometric cross section of the particles, and Q_{sca} represents the scattering efficiency of the particles.

Finally, the Fresnel's equations explain the attenuation of the refracted ray when the light moves from a medium to another with a different refractive index. According to the Fresnel's law, part of the light is refracted and part of it is reflected at the boundary between the media. We define $\mathcal{L}_{bound}$ as the boundary attenuation, and as it can be seen in Fig. 2, this attenuation happens twice. Once when the light enters the sphere and once when it moves out. The behavior depends on the polarization of the incident ray, which can be separated into 2 cases of s- and p-polarized. R_s and R_p are defined as the reflectance of the s- and p-polarized lights respectively, and are given as follows for the ingoing light:

$$R_{s,i} = \left|\frac{n_{1,r}cos(\theta_i) - n_{2,r}cos(\theta_r)}{n_{1,r}cos(\theta_i) + n_{2,r}cos(\theta_r)}\right|^2, \quad (13)$$

$$R_{p,i} = \left|\frac{n_{1,r}cos(\theta_r) - n_{2,r}cos(\theta_i)}{n_{1,r}cos(\theta_r) + n_{2,r}cos(\theta_i)}\right|^2, \quad (14)$$

where $R_{s,i}$ and $R_{p,i}$ are the reflectance of the s- and p-polarized ingoing lights respectively (Fig. 3). Following the same type of equations, one can find the reflectance of the outgoing lights named $R_{s,o}$ and $R_{p,o}$ for the s- and p-polarized waves respectively. The transmittance of the light $T_{s/p,i/o}$ is given as $T_{s/p,i/o} = 1 - R_{s/p,i/o}$. In the special case of the main ray where $\theta_i = \theta_r = \theta_o = 0$, the reflectance is given by:

$$R^{mr} = \left|\frac{n_{1,r} - n_{2,r}}{n_{1,r} + n_{2,r}}\right|^2. \quad (15)$$

Hence the boundary loss for the main ray is $\mathcal{L}^{mr}_{bound} = (T^{mr})^2$, where T^{mr} is the transmittance of the main ray and is equal to $1 - R^{mr}$. The boundary loss of a secondary ray which forms a plane of incident (containing the incident, reflected and refracted rays) and has the angle θ with the x axis, is $\mathcal{L}^{fr,s}_{bound} = T_{s,i}T_{s,o}$, and $\mathcal{L}^{fr,p}_{bound} = T_{p,i}T_{p,o}$, where $\mathcal{L}^{fr,s}_{bound}$ and $\mathcal{L}^{fr,p}_{bound}$ are the boundary losses for the s- and p-polarized parts of a secondary ray respectively.

Fig. 3 shows the cross section of the sphere cell on the xy plane. Note that the polarization of the wave is along the x

$$\vec{E}_F^{fr}(\alpha) = \left|\vec{E}_0\right| \Big(\mathcal{L}^{fr,p} \int_0^{2\pi} cos^2(\theta)cos(\psi)\hat{a}_x + sin(\theta)cos(\theta)cos(\psi)\hat{a}_y + cos(\theta)sin(\psi)\hat{a}_z d\theta + \mathcal{L}^{fr,s} \int_0^{2\pi} sin^2(\theta)\hat{a}_x - sin(\theta)cos(\theta)\hat{a}_y d\theta \Big). \tag{12}$$

axis and the direction of the propagation is along z axis. We solve the problem for an arbitrary secondary ray in a plane of incident and then integrate the results over all the planes of incidents by covering θ from zero to 2π, where θ is the angle between the plane of incident and x axis in spherical coordinates. To find the light intensity E_F at a given focal point with parameter α, we start with from all the secondary rays that are focusing at a point as follows:

$$\vec{E}_F^{fr}(\alpha) = \int_0^{2\pi} \vec{E}_F^{ray}(\alpha, \theta) d\theta, \tag{16}$$

where $\vec{E}_F^{fr}(\alpha)$ is the total received field from all the secondary rays that are focusing at the focal point with the distance $r \cdot f(\alpha)$ from the center of the cell. $\vec{E}_F^{ray}(\alpha, \theta)$ is the intensity of a single secondary ray at the aforementioned point which is coming through the plane of incident that forms the angle θ with the axis x (Fig. 3), and is given by:

$$\vec{E}_F^{ray}(\alpha, \theta) = \mathcal{L}_{abs}\mathcal{L}_{sca}\Big(\mathcal{L}_{bound}^{fr,p}\vec{E}_{0p} + \mathcal{L}_{bound}^{fr,s}\vec{E}_{0s}\Big), \tag{17}$$

Where $\vec{E}_{0p}$ and $\vec{E}_{0s}$ are the p- and s-polarized parts of the incoming ray $\vec{E}_0$ as shown in Fig. 3, and are given by:

$$\vec{E}_{0p} = \left|\vec{E}_0\right| cos(\theta)\hat{a}_p, \quad \vec{E}_{0s} = \left|\vec{E}_0\right| sin(\theta)\hat{a}_s, \tag{18}$$

where $\hat{a}_p$ and $\hat{a}_s$ are the unit vectors in the direction of $\vec{E}_{0p}$ and $\vec{E}_{0s}$ and are given by $\hat{a}_p = cos(\theta)\hat{a}_x + sin(\theta)\hat{a}_y$ and $\hat{a}_s = sin(\theta)\hat{a}_x - cos(\theta)\hat{a}_y$ respectively. By substituting the equations (18) and (17) in (16), and considering the final refracted angle of a focal ray ψ as shown in Fig. 2, equation (16) can be rewritten as the equation (12) -on top of the page-, where $\mathcal{L}^{fr,p}$ and $\mathcal{L}^{fr,s}$ represent the path loss that every p- and s-polarized focusing ray faces in its path to the focal point and are equal to $\mathcal{L}_{abs}\mathcal{L}_{sca}\mathcal{L}_{bound}^{fr,p}$ and $\mathcal{L}_{abs}\mathcal{L}_{sca}\mathcal{L}_{bound}^{fr,s}$ respectively.

It can be easily observed that the answer of the integral is equal to zero in the y and z directions. Hence the aggregated field coming from the secondary rays is further simplified to:

$$\vec{E}_F^{fr}(\alpha) = \pi\left|\vec{E}_0\right| (\mathcal{L}^{fr,p}cos(\psi) + \mathcal{L}^{fr,s})\hat{a}_x. \tag{19}$$

Note that interestingly $\vec{E}_0$ is also considered to be polarized along the x axis and hence propagating through z direction. Following the same approach the received field coming through the main ray over the focal line can be also given as:

$$\vec{E}_F^{mr} = \left|\vec{E}_0\right| \mathcal{L}^{mr}\hat{a}_x, \tag{20}$$

where $\mathcal{L}^{mr}$ is the path loss that the main ray faces in its path to a point on the focal line. Now that we have all the information for the path loss and delay, the channel impulse response on the focal line between the points f_l and f_u can be given as:

$$H(f, d) = \left|\vec{E}_F^{mr}\right| e^{-j\omega\tau_{mr}} + \left|\vec{E}_F^{fr}\right| e^{-j\omega\tau_{fr}}, \tag{21}$$

where $\gamma(r)$ is the cell-size gain factor which is a function of the radius of the cell. The larger the cell, the bigger the surface of the cell that is being exposed to the incoming light, and hence the more energy will be focused at the focal line. In equation (21), d is the total distance between the light source and the point on the focal line and is considered to belong to the interval $d \in l_0 + [r(1+f_l)\ \ r(1+f_u)]$, for the equation to be valid. It can be observed, that for a given l_0, the value of α can be calculated from d. Note that E and τ are functions of f and d (or equivalently α), and we consider the normalized channel impulse response for which $\left|\vec{E}_0\right|$ is assumed to be equal to one. Furthermore, there is no time difference between the secondary rays with the same angle of incident θ_i or equivalently α, so that we can do the integration without considering the time, and then we will add the time delay for the final expression of $H(f, d)$ which contains both the main and secondary rays that are received with different time delays.

IV. Results and Discussion

The theoretical model is validated by simulating the electromagnetic wave propagation using COMSOL Multiphysics. All the parameters used in FEM simulations are the same as those in analytical model. The blood vessel is modeled as a medium containing cytoplasm and RBCs. The relative permittivity for cytoplasm, fat, and hemoglobin at certain wavelengths are taken from experimental measurements [9], [15]. It is considered that the size of each cell is in the range of (1.5–3)λ, with $\lambda = 600$ nm. The distance of the antenna with the boundary of the cell for the single cell scenario is considered to be (7)λ. For both the simulation and analytical model, a plane wave excitation has been considered.

Fig. 4 shows the intensity of light while propagating through a single RBC with (a) $r = 1.5\lambda$, (b) $r = 3\lambda$, and (c) blood plasma without any cells. Simulation results show that the intensity of light is amplified after the cell and focused on the central line that passes through the center of cell (focal line).

The intensity of the light over the focal line which has been derived from the analytical channel model is compared to the simulation results in Fig. 5. The slight difference can be explained by scattering of the light in the medium from the sides of the cell and the effect of the tiny fat layer that has not been captured with the analytical model. However, as

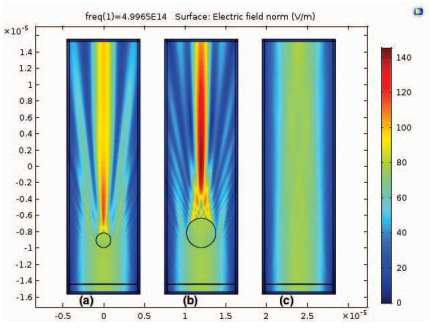

Fig. 4. Electric field intensity after one RBC illuminated with port antenna (a) $r = 0.9\ \mu m$ (b) $r = 1.8\ \mu m$ (c) no cell.

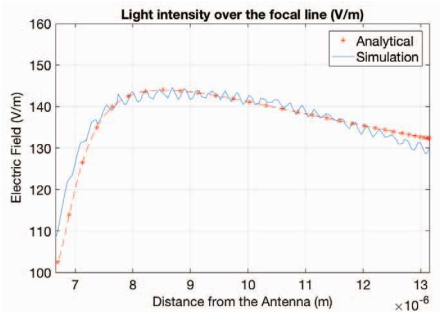

Fig. 5. Electric field intensity on focal line, analytical vs simulation results.

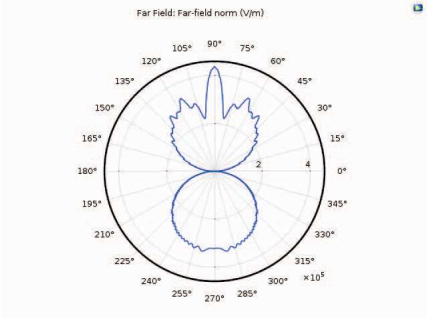

Fig. 6. Polar plot of Electric field intensity around one RBC with $r = 0.9\ \mu m$.

it can be seen in this figure, the theoretical model is accurate enough to be used for modeling the optical wireless channel in terms of the path loss and time delays. Interestingly there is a point on the focal line in which the amplification is maximal. This happens at the Brewster's angle which causes the minimal boundary loss while light passes from one medium to another with different refractive indexes.

As depicted with a polar plot in Fig. 6, most of the light is forwardly scattered which is in agreement with the Mie theory of scattering. Also, behind the cell the total field is slightly changed due to the backscattered light from the fat layer, but is almost the same as the field radiated from the antenna.

Finally simulation results for the case of multiple cells positioned randomly inside the blood plasma is shown in Fig. 7. It can be seen that while in (a) the light is significantly amplified at some rays at the end of the path, in (b) the light intensity stays almost the same for the entire path.

V. Conclusions

In this paper, we have developed a channel model for *in vivo* optical communication in iWNSNs. In particular, a geometrical approach has been followed to trace path loss and time delay of each of the rays that encounter a biological cell. A closed form channel impulse response on the focal line has been derived by aggregating all the rays while considering the attenuation and delay of each of them. We have shown that after passing a single RBC, all the optical rays will be focusing on the central line. The results show that the path loss for the communication through the RBCs inside the blood is lowered, which is achieved by the intrinsic focusing capability of the RBCs that are performing as optical micro-lense. Moreover, simulations and recent experimental studies show that the obtained model in this paper is accurate enough to model the intra-body optical channel for a single cell. In addition, the propagation pattern that has been derived here for a single cell

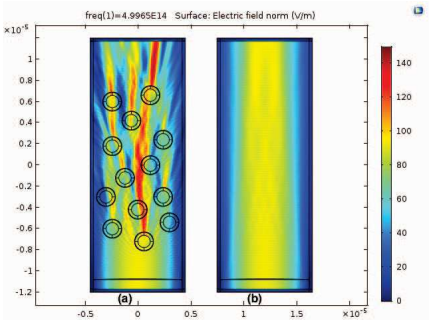

Fig. 7. Electric field propagation pattern after multiple randomly placed RBCs illuminated with port antenna (a) with cells (b) without cells.

can be used as the building block to pave the way to achieve a more complicated channel model including numerous cells of different types in multiple layers.

Acknowledgments

This work was supported by the U.S. National Science Foundation (NSF) under Grants No. CBET-1445934 and No. CBET-1555720.

References

[1] R. Renault, N. Sukenik, S. Descroix, L. Malaquin, J.-L. Viovy, J.-M. Peyrin, S. Bottani, P. Monceau, E. Moses, and M. Vignes, "Combining microfluidics, optogenetics and calcium imaging to study neuronal communication in vitro," *PloS one*, vol. 10, no. 4, p. e0120680, 2015.

[2] F. Schmid, L. Wachsmuth, M. Schwalm, P.-H. Prouvot, E. R. Jubal, C. Fois, G. Pramanik, C. Zimmer, C. Faber, and A. Stroh, "Assessing sensory versus optogenetic network activation by combining (o) fmri with optical ca2+ recordings," *Journal of Cerebral Blood Flow & Metabolism*, p. 0271678X15619428, 2015.

[3] M. Khajavikhan, A. Simic, M. Katz, J. Lee, B. Slutsky, A. Mizrahi, V. Lomakin, and Y. Fainman, "Thresholdless nanoscale coaxial lasers," *Nature*, vol. 482, no. 7384, pp. 204–207, 2012.

[4] J. M. Jornet and I. F. Akyildiz, "Graphene-based plasmonic nano-antenna for terahertz band communication in nanonetworks," *IEEE Journal on selected areas in communications*, vol. 31, no. 12, pp. 685–694, 2013.

[5] L. Tang, S. E. Kocabas, S. Latif, A. K. Okyay, D.-S. Ly-Gagnon, K. C. Saraswat, and D. A. Miller, "Nanometre-scale germanium photodetector enhanced by a near-infrared dipole antenna," *Nature Photonics*, vol. 2, no. 4, pp. 226–229, 2008.

[6] I. F. Akyildiz, F. Brunetti, and C. Blázquez, "Nanonetworks: A new communication paradigm," *Computer Networks*, vol. 52, no. 12, pp. 2260–2279, 2008.

[7] M. Pierobon and I. F. Akyildiz, "Capacity of a diffusion-based molecular communication system with channel memory and molecular noise," *IEEE Transactions on Information Theory*, vol. 59, no. 2, pp. 942–954, 2013.

[8] J. Dorfmuller, R. Vogelgesang, W. Khunsin, C. Rockstuhl, C. Etrich, and K. Kern, "Plasmonic nanowire antennas: experiment, simulation, and theory," *Nano letters*, vol. 10, no. 9, pp. 3596–3603, 2010.

[9] R. M. Pope and E. S. Fry, "Absorption spectrum (380–700 nm) of pure water. ii. integrating cavity measurements," *Applied optics*, vol. 36, no. 33, pp. 8710–8723, 1997.

[10] S. L. Jacques, "Optical properties of biological tissues: a review," *Physics in medicine and biology*, vol. 58, no. 11, p. R37, 2013.

[11] L. V. Wang and H.-i. Wu, *Biomedical optics: principles and imaging*. John Wiley & Sons, 2012.

[12] J. C. Lin, *Electromagnetic fields in biological systems*. CRC press, 2011.

[13] H. Guo, P. Johari, J. M. Jornet, and Z. Sun, "Intra-body optical channel modeling for in vivo wireless nanosensor networks," *IEEE transactions on nanobioscience*, vol. 15, no. 1, pp. 41–52, 2016.

[14] L. Miccio, P. Memmolo, F. Merola, P. Netti, and P. Ferraro, "Red blood cell as an adaptive optofluidic microlens," *Nature communications*, vol. 6, 2015.

[15] S. Prahl, *Oregon Medical Laser Center*, 1999. [Online]. Available: http://omlc.org/spectra/hemoglobin/summary.html